

Use of a Microphone Phased Array to Determine Noise Sources in a Rocket Plume

J. Panda*

NASA Ames Research Center, Moffett Field, CA

R. Mosher

Aerospace Computing, Inc, Mountain View, CA

Abstract

A 70-element microphone phased array was used to identify noise sources in the plume of a solid rocket motor. An environment chamber was built and other precautions were taken to protect the sensitive condenser microphones from rain, thunderstorms and other environmental elements during prolonged stay in the outdoor test stand. A camera mounted at the center of the array was used to photograph the plume. In the first phase of the study the array was placed in an anechoic chamber for calibration, and validation of the indigenous Matlab® based beamform software. It was found that the “advanced” beamform methods, such as CLEAN-SC was partially successful in indentifying speaker sources placed closer than the Rayleigh criteria. To participate in the field test all equipments were shipped to NASA Marshal Space Flight Center, where the elements of the array hardware were rebuilt around the test stand. The sensitive amplifiers and the data acquisition hardware were placed in a safe basement, and 100m long cables were used to connect the microphones, Kulites and the camera. The array chamber and the microphones were found to withstand the environmental elements as well as the shaking from the rocket plume generated noise. The beamform map was superimposed on a photo of the rocket plume to readily identify the source distribution. It was found that the plume made an exceptionally long, >30 diameter, noise source over a large frequency range. The shock pattern created spatial modulation of the noise source. Interestingly, the concrete pad of the horizontal test stand was found to be a good acoustic reflector: the beamform map showed two distinct source distributions- the plume and its reflection on the pad. The array was found to be most effective in the frequency range of 2kHz to 10kHz. As expected, the classical beamform method excessively smeared the noise sources at lower frequencies and produced excessive side-lobes at higher frequencies. The “advanced” beamform routine CLEAN-SC created a series of lumped sources which may be unphysical. We believe that the present effort is the first-ever attempt to directly measure noise source distribution in a rocket plume.

I. INTRODUCTION

Significant advancements in the sensor, data acquisition and computing technologies, as well as the recent progress in sharpening the noise source distribution via advanced processing techniques, have widened the usage of microphone phased array in recent years. The aircraft industry heavily uses phased array for the identification of noise sources on airframes, engines, landing gears and other parts of an aircraft^{1, 2, 5, 9, 10}. Arrays are used to detect noise sources in automotive and manufacturing industries. The goal of the present work is to extend the usage of this technology for spacecraft applications. The present paper reports on the application of a suitably tailored phased array in establishing the noise sources in a solid rocket plume. Towards this end an existing 70 elements array was modified for high-noise, outdoor, all-weather application; an easily transportable data acquisition and processing system was assembled, and new processing codes are written to take advantage of the newer deconvolution procedures. The ultimate goal of the present work is to use a microphone phased array for the launch acoustics application.

II. FUNDAMENTALS OF THE PHASED-ARRAY BEAMFORMING

Fundamentally a phased array images the sound sources by analyzing the phase front of the waves sensed by a large number of microphones. The individual microphone signals are delayed in time (or equivalently, in phase) and then added together. The first step in the imaging process is to divide the spatial zone (where the sound

* Associate Fellow, AIAA

sources lay) into a large number of grid points, which are called the interrogation points. If there lays a noise source in one of the grid points, then the estimated time delays (phase differences) for sound waves to reach the microphones are correct, and the summing process gives a large output. On the other hand if the interrogation point is not a noise source then the final sum is much lower. This simple principle makes what is known as the conventional beam forming, whereby a beamformed map is created over the interrogation region.

A downside of this process, especially for the low frequency end, is that the summed-up array output decreases slowly from the locations of the actual source to the neighboring regions. Additionally there may appear multiple local maxima (side lobes) which may give the appearance of pseudo noise sources. These difficulties are from the diffraction characteristics of the array, and are dictated by the design of the microphone layout. This fundamental property of the array response is described by its point-spread-function, PSF (Fig 1b). As the name implies, a point-spread-function describes how a point source becomes spread out in the beamform map. Even the best possible layout can only try to reduce the side lobes. The smearing of the actual source location is directly proportional to the frequency of interest: worst for the lowest frequency while improving with an increase in frequency. However, the strength and number of side lobes (that falsely makes the appearance of adjacent sources) is inversely proportional to the frequency. In a nutshell the classical beamform suffers from poor resolution due to the inherent instrument function.

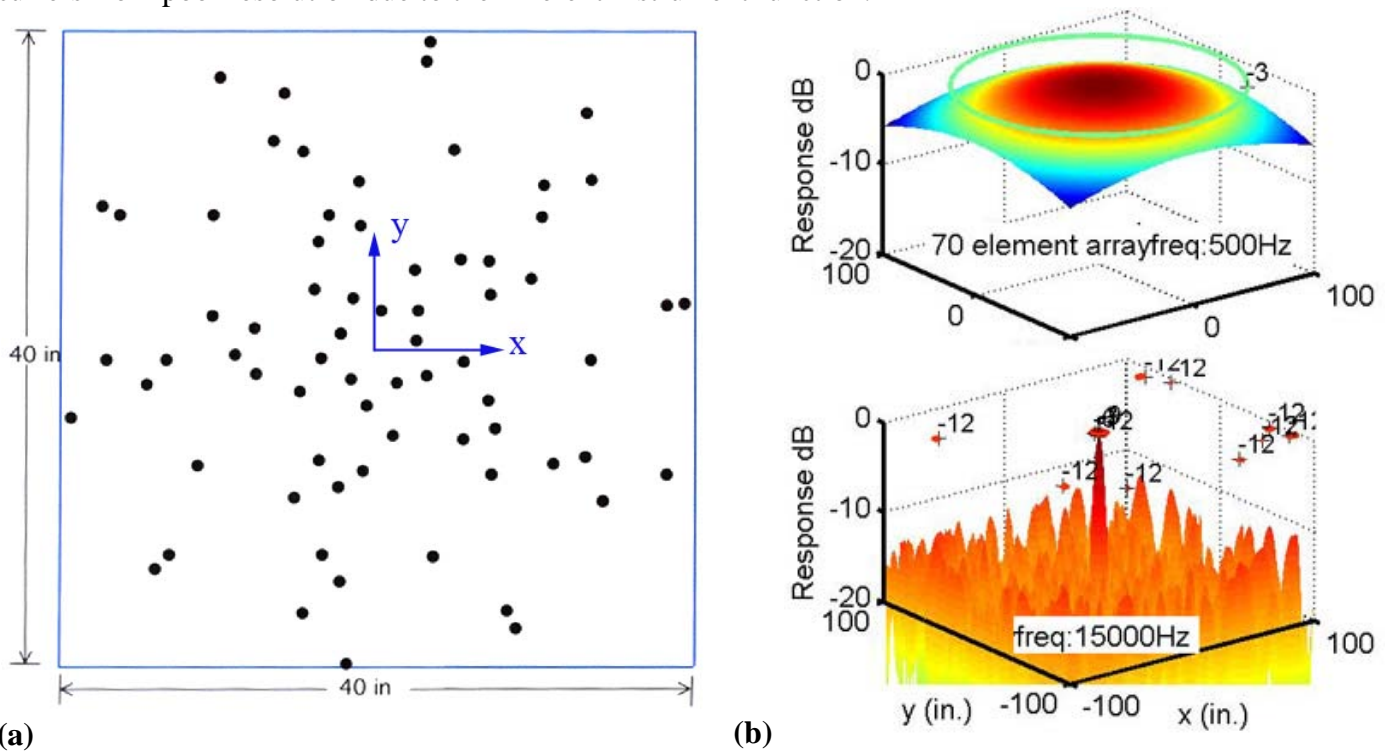


Fig. 1. (a) Microphone pattern on the array plate; (b) point spread function (PSF) for the two indicated frequencies for a point source located at the origin and $z = 240$ inches away from the plate.

In the recent times there have been multiple efforts to improve the array resolution by deconvolving the point-spread function from the beamformed output. The most straightforward one DAMAS¹ involve large matrix manipulation and very long computing time. There are multiple clever approaches^{1, 2, 3} with their own shortcomings. One of the better approaches: CLEAN-SC^{1, 2} is employed for the current analysis. In the following, mathematical steps for the conventional and CLEAN-SC beamforming are outlined.

IIa. Conventional beamforming (CB):

Let ξ_j : $j=1, 2, 3, \dots, N$ are the interrogation points in the region containing the noise source(s), and a phased-array that contains $\ell = 1, 2, \dots, M$ no of microphones is used for the test. The radial distance from an interrogation point to an individual microphone $r_{j\ell}$ determines the phase shift and the relative amplitude measured by the microphone. The steering vector is a $[M \times 1]$ column matrix defined to incorporate these properties:

$$\text{---} \quad (1)$$

Where χ is a constant to normalize the steering vectors: $\frac{1}{\sqrt{2\pi}}$, and β : acoustic wavenumber $\frac{2\pi}{\lambda}$, f : frequency, c : speed of sound. The \dagger symbol represents a complex-conjugate and transpose operation. The above equation is valid if the noise source radiates as a monopole. This basic assumption of the beamforming process has been under scrutiny for the entire history of the phased- array technology. The justification for the assumption has been that little change in the beam-formed map is obtained by assuming other type of sources. Besides, in a lift-off environment there exist a variety of distributed noise sources and many reflective surfaces. The possibility of making bad error is minimized by assuming that the noise sources are made of an agglomeration of multitudes of monopoles.

The time traces of pressure fluctuations from individual microphones are Fourier transformed to obtain individual spectra $P_i(f)$. The cross-spectra between every pair of microphones are calculated and stored in a cross-spectral matrix \mathbf{G} . Every element of the cross-spectral matrix (CSM) is calculated as:

(2)

The $*$ represents a complex conjugate, and the $\langle \cdot \rangle$ represents expected value i.e. a time average over several seconds. Typically the Fourier transform is performed over multiple overlapping blocks of data which are then multiplied using the above equation and finally averaged to obtain individual elements of the CSM. The diagonal elements of the CSM G_{11} , G_{22} , G_{33} , etc. contain the auto-spectra which are contaminated by various spurious noise sources, such as that from the electronic noise and, in wind tunnel environment, from the turbulent boundary layer present over the array plate. Zeroing out the diagonal elements improves the beamformed map; although some of the amplitude information become lost.

The summing of the microphone signals, i.e. the elements of cross-spectral matrices, needs to be preceded by a phase adjustment. These two steps are combined in a matrix manipulation which leads to the beamform map:

(3)

IIb. Deconvolution using CLAEAN-SC:

As discussed earlier, the source map obtained via the conventional beamform process has poor resolution at low frequency range, and the presence of many side-lobes in the high frequency range. These artifacts are due to the smearing and interference associated with the point-spread-function (PSF) inherent to the array lay-out. However, the PSF at any point k in the beamformed region can be predetermined:

(4)

The CLEAN-Spatial Correlation is a relatively fast and well-understood methodology among many available procedures to remove the influence of the PSF on the source map. It ought to be understood that one needs to trace the presence of the source in the conventional map before applying any of the deconvolution procedures. The deconvolution processes work on the conventional map to sharpen the location of the source and to help eliminate the side-lobes.

CLEAN-SC is an improvement over the original CLEAN methodology that is used in radio astronomy. The name CLEAN comes from the progressive buildup of a “clean-map” C^i in the expense of a “dirty-map” D^i . Initially, the dirty map is the conventional beamform:

(5)

The process begins with the identification of the location ξ_k and level b_{kk} of the peak noise source in the conventional beamform. The clean map C^i is started with this location and level:

(6)

Here α is a smearing factor, without which the sharp peaks may not be detectable in the plots. Next the expected contribution of an equivalent monopole (of strength b_{kk} located at ξ_k) is subtracted out from both the CSM and the dirty map. The peak locations and levels in this revised dirty map are transferred to the clean map. The process is continued till a convergence criterion is met.

Peter Sijtsma’s contribution in CLEAN-SC⁵ is an improved procedure to subtract out contribution of the already found source at the peak location. The procedure is based upon the coherence values between the peak source b_{kk} at location ξ_k with all other points in the beamformed map. Quintessentially the point-spread-function makes the influence of a point source ‘felt’ over the entire beamform map. This spread-out part is established

via the coherence levels between the source at ξ_k and all other points ξ_j in the map. However, that coherence calculation depends on whether the diagonal terms of the CSM are deleted or not.

When *the diagonal elements of the CSM are as measured (not deleted)*, the coherence is calculated based on the degraded CSM as:

$$\text{---} \quad (7)$$

The new degraded dirty-map is calculated by subtracting out the coherent part from the earlier version:

$$(8)$$

The degraded CSM is then established by factoring out contribution of an equivalent monopole at ξ_k :

$$(9)$$

The convergence is achieved when the newly degraded CSM has more energy than the previous iteration:

$$(10)$$

The Final clean map is simply a sum of peaks found in the earlier iteration plus the final degraded dirty-map:

$$(11)$$

When *the diagonal elements of the CSM are deleted* the coherence value Γ^2 can become unphysical, since the beamform values b_{jj} can even be negative. Equations (7), (8) & (9) cannot be applied anymore. Instead of directly calculating the coherence (which was ultimately used to establish the degraded CSM, equation 9), Sijtsma specifies an effective steering vector \mathbf{h} from the source point ξ_k :

$$\text{---} \quad (12)$$

which is then used to establish the degraded CSM:

$$(13)$$

In the above two equations \mathbf{h} is calculated iteratively starting with an initial value of $\mathbf{h} = \mathbf{w}_k$. The converged \mathbf{h} values are obtained within a few iterations. Unlike the equation (8) above the degraded dirty-map is calculated from the degraded CSM:

$$\text{---} \quad (14)$$

which is then used to find out the new peak. The process is continued till the convergence criterion of equation (11) is met. Typically an acceleration factor (between 0.5 and 0.95) is used to help extract distributed sources with equations (8), (9) & (13).

IIc. Matlab® implementation:

The above beamforming schemes are implemented in the commercially available Matlab® platform. A quad-core Personal Computer is used along with the Matlab® Distributed Computing Toolbox. Once the cross-spectral matrix is calculated the rest of the beamforming operation happens fairly quickly (few seconds for each frequency bins). The CSM calculation may take anywhere between one to five minutes, depending on the duration of the microphone data.

To facilitate direct identification of the noise sources, the interrogation grid for beamforming is created over a photograph of the region of interest. A video camera is mounted at the center of the array which is used to capture 7.5 frames per sec video simultaneously over the duration of the microphone data recording. When the noise source is stationary only one frame of the captured video is sufficient for further processing. The first step after selecting the frame is to perform a correction for barrel distortion due to the fish-eye lens used with the camera. The low focal length lens is useful to capture a large view angle. The correction factor a ($s = r + ar^3$, s : true radius, r : measured radius of each pixel from the center of the image) is obtained by trial and error. In the next step the photographed region was divided into a uniformly spaced grid. To select the number of grid points, Rayleigh criterion is applied to the highest frequency of interest. According to this criterion the minimum resolvable detail is due to the diffraction-limit of the array when the first diffraction minimum of the image of one source point coincides with the maximum of another. For a circular aperture of diameter d , the Rayleigh resolution in radian θ_R is as following:

$$\text{---} \quad (15)$$

Typically the grid spacing obtained using the above equation is refined by a factor anywhere between 4 and 10. The higher the factor the slower is the processing.

The cross-spectral matrix (CSM) of equation 2 is calculated as soon as the data is collected. Once computed the information can be used with any number of schemes and beamforming choices without a need for recalculation. In the next step the conventional beamforming was performed (equation 3) followed by DAMAS2 (see reference 6) and CLEAN-SC (equation 11). Subsequently, the beamformed colored maps are superimposed on the video image for direct identification of the noise sources. There exist a quick-look and a detailed analysis version of the code. The former analyzes only four selected frequencies, while the latter is for overnight processing of all narrowband frequencies (typically 512). The narrowband beamformed data can be combined for third octave presentations.

III. ARRAY HARDWARE:

The 70-element microphone array was designed for earlier wind tunnel tests. Burnside et al¹ described the array design, followed by test results from an airframe noise test by Horne et al¹⁰. The outdoor rocket firing represented a challenging environment that required a different approach for mounting and protecting the basic array plate. Besides, the array plate was modified to place a video camera at the center, and two dynamic pressure transducers (Kulite) to measure impulse loading from Ignition Over Pressure (IOP) pulse. The video camera was used to directly image the physical noise sources. A wide-angle 3.5mm lens was used with the camera to cover a large spatial region.

The restricted access to the test stand with a live motor meant that the array had to be in place nearly a week before the firing. An “environment chamber” was built around the plate to protect the sensitive equipments from rain, snow, wind and other elements. The chamber was made of three components: a cover plate for the front end, a back-chamber to protect the rear end, and two junction boxes, attached to the back-chamber, to make water-tight connection for the large number cables. The environment chamber, made of aluminum frame, sheet metal and polycarbonate boards, was sealed using weather strips and silicone sealants. The rear chamber also held desiccants to maintain a dry environment. However, during a simulated rain test it was found that the chamber was not completely water proof. This led to an addition of two more preventive measures. A large plastic bag was placed over the whole environment chamber, and the rear chamber was continuously purged using very dry missile grade air. These four preventive measures were found to be effective through subsequent rain tests (Figure 2a) and ultimately during the two-week exposure at the test site when several thunderstorms passed over the array hardware (figure 2b).

The array was placed 15 feet away from the nozzle centerline, in the nozzle exit plane. The primary reason for that location was to avoid interference with all other pole mounted microphones and IOP sensors used in the test. The array bottom edge was elevated 2 feet above the ground surface, and the array itself was rotated about its y-axis by 30°, so that the camera had a clear view of the entire plume. A line normal to the array surface (i.e. the z-axis in the array coordinate) made a 30° angle to the plume axis.



Fig. 2(a) Simulated rain test on the environment chamber (covered by a plastic wrap) at NASA ARC to verify water-proofing.

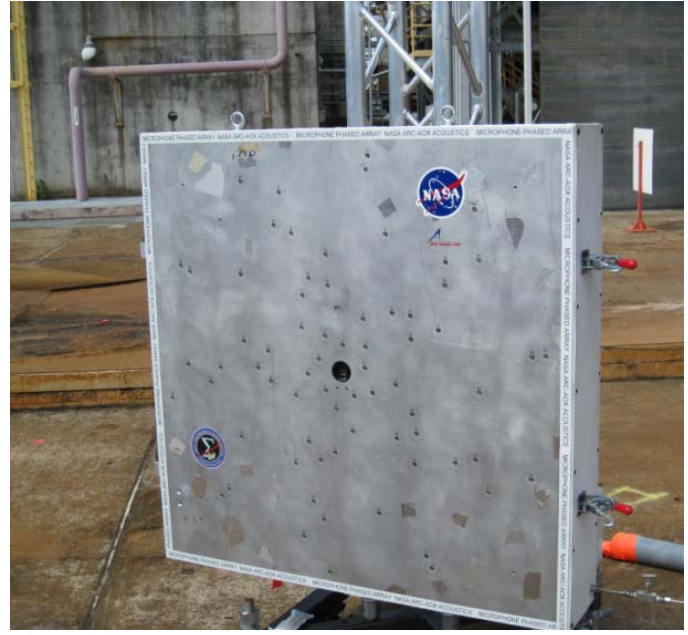


Fig. 2(b) Array setup at NASA MSFC. Note that the small tube at bottom right provided a dry air purge to the array chamber.

All other electronic equipments (microphone amplifiers, data acquisition system, computer etc) were placed indoor in an air-conditioned basement away from the test stand. 100 meter long cables were used to connect microphone preamplifiers to the amplifiers. At the array chamber the cables were passed through several rubber grommets at the junction-box to make water-tight connections with the pig-tail cables from the preamplifiers. The long cable bundle was protected by split PVC pipes. A 72 channel, 16bit VXI system was used for simultaneous acquisition of the microphone signal. The Personal Computer interfacing with the DAQ system was accessed over a local network from the nearby control room. The same PC was used for capturing video signal from the array-camera which was connected via a Fireware® extender. The data acquisition was started at $t-10$ count and lasted for 30 sec with a sampling rate of 51200/sec. The actual motor burn lasted for about 6 seconds, out of which the first 2 sec was the full-power burn. Data from the full-power burn was used for source identification. Later analysis showed that the array plate was subjected to IOP wave of ~ 0.6 psi pressure rise and 145dB acoustic level. All microphone and Kulite sensors were found to be intact at the end of the test. The only casualty was a neutral density filter that was loosely mounted in front of the camera. It fell down wasting most of the video footage.

IV. RESULTS AND DISCUSSIONS

IVa. Validation from setup in an anechoic chamber:

The initial checkup, calibration and software validation were performed in the NASA Ames Acoustics laboratory. The array was mounted inside an anechoic chamber (Fig. 3a). A vertical truss structure, similar to the one to be used in the field test, was used to mount the array plate. At first the camera was calibrated to associate spatial position with the individual pixels. This was followed by an end-to-end calibration of individual microphone using a Piston phone. Finally, a large number of validation data were obtained by placing a set of three speakers and driving them using separate broadband white noise generators. Following are some sample results that provide a comparison between various beamforming schemes.

For Figs (4) the three speakers were equally spaced at 31 inches and positioned at $z = 176$ " from the array center. The beamform-map is superimposed on a video frame to help identify individual sources. The "drawn curtain" appearance of the image is due to the correction applied to remove barrel distortion. There are four columns of plots for four different narrow-band frequencies, and three rows for three different beamforming methodologies. An examination of the top row of figures shows that the array along with the conventional beamforming is unable to resolve individual speakers at the two lower frequencies, while they are

correctly identified at the two higher frequencies. At the highest 15 kHz frequency a large number of side lobes appear which makes the appearance of pseudo-sources. It is interesting to note that Rayleigh criterion of equation (15) places the minimum resolvable frequency at around 2300 Hz for the speaker positions (the equivalent circular aperture of the array is assumed to be 40 inches). The top row of figure 4 seems to provide support to this criterion.

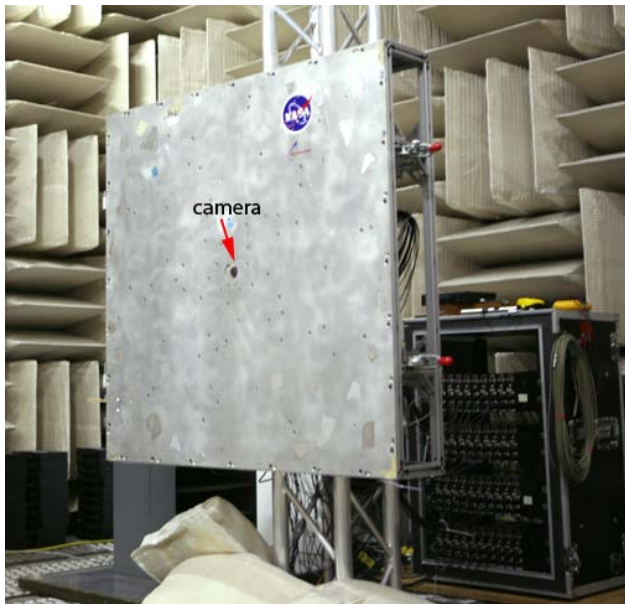


Fig 3(a). Phased-array inside an anechoic chamber.

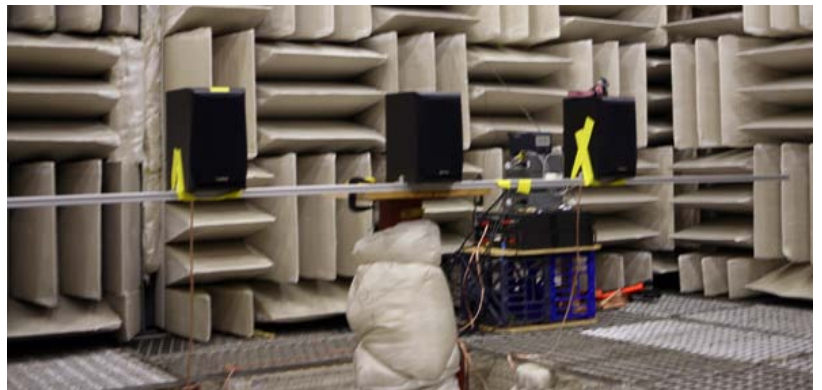


Fig 3(b). Speaker arrangement to test the array operation.

The conventional beamform data were further analyzed using two deconvolution methods: DAMAS⁶ and CLEAN-SC⁵; the latter one was discussed earlier. The bottom two rows of figure 4 show result from the application of these methods. The deconvolution routines significantly localize the source; CLEAN-SC making a superior job in eliminating the effect of the point-spread-function. However neither can isolate the three speakers at the lower frequencies below the Rayleigh resolution limit. A closer look into the methodologies clarifies this deficiency. The deconvolution procedures start with the peak noise identified in the conventional map (equation 6 above). The location and level of the peak are due to a sum of effects from all three sources. For frequencies below the Rayleigh resolution, the peak in the conventional beamform does not coincide with a speaker location. This makes the deconvolution procedure to start with an incorrect assumption of the peak noise source that ultimately led to incorrect distribution of sources. Fundamentally, for sources spaced closer than the Rayleigh resolution, the summed up field may not have a unique solution for noise sources; that is, multiple combination of locations and amplitudes may provide the same final distribution. Therefore, it is believed that the limitation imposed by the Rayleigh criterion is difficult to overcome by the above deconvolution procedures. For frequencies higher than the Rayleigh resolution, figure 4 shows that the deconvolution procedures significantly reduce side lobes and dramatically improve beamform results, at least for the point source in an ideal anechoic environment.

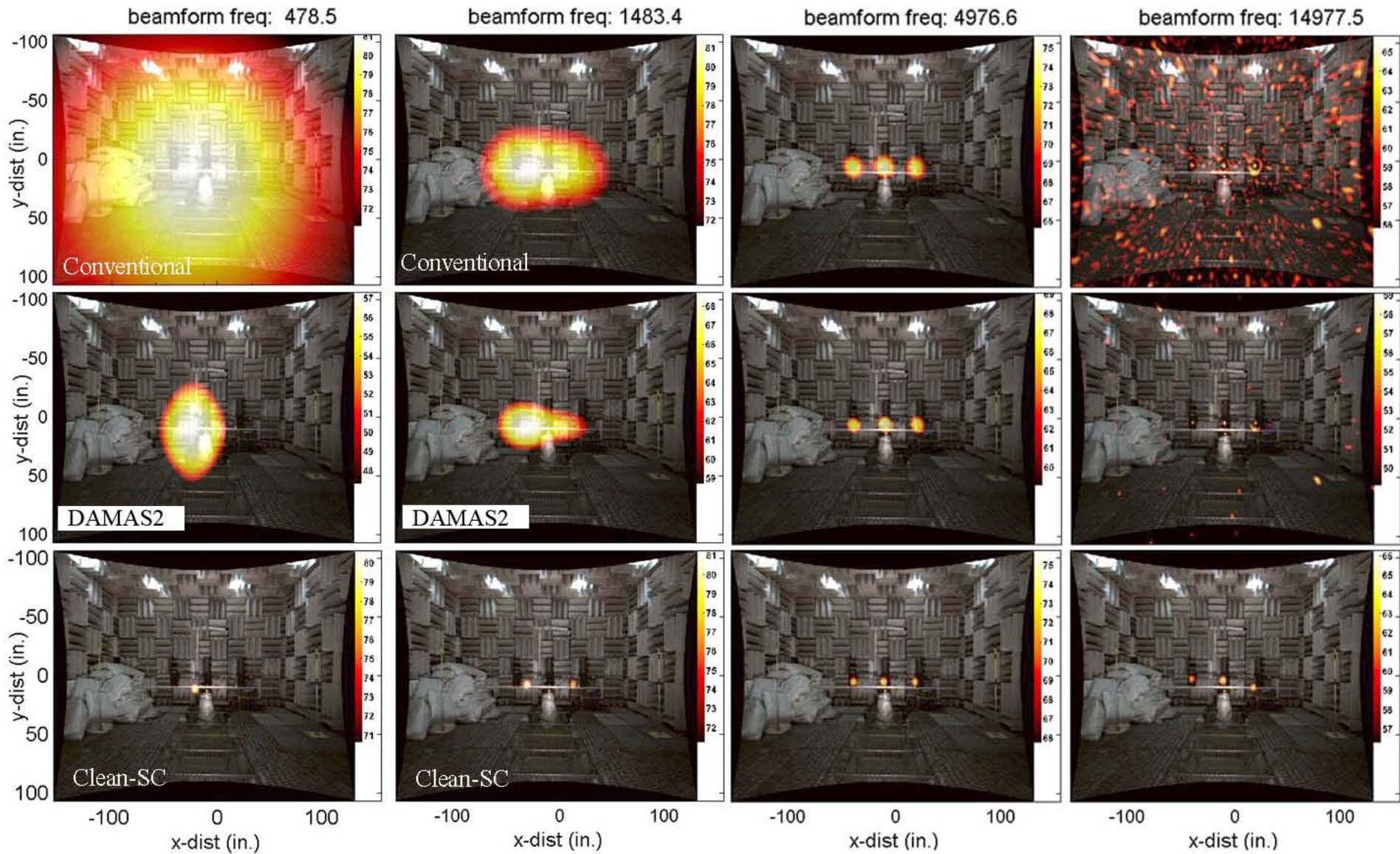


Fig 4. A comparative study of beamforming at the indicated frequencies via the three indicated methods.

IVb. Source identification in the plume of a Solid Rocket Motor:

After the completion of the validation test in the Ames anechoic chamber, the environment chamber was added to the array plate and, along with all electronics and mounting structures, shipped to NASA Marshall. There the entire system was assembled, calibrated and validated. The setup used in the horizontal test stand is shown in figure 5. The camera at the center of the array plate captured a better image of the plume; although only one frame in the video was useful (Fig. 6). This frame, from the very start of the burn, shows clear periodic shock pattern present in the under-expanded plume. The glow in the plume is due to afterburning. The smoke is believed to be mostly made of Aluminum Oxide powder. The three vertical lines are the poles used for holding microphones for a separate suit of instrumentations.

Figure 7 shows a sample time trace, auto- and cross- spectra collected from the test. Noticeably the 1/3 rd octave spectrum have double hump, separated by a dip which are indicative of acoustic interference from distinct sources.

Conventional beamform results at four different frequencies are shown in figure 8. The color plot covers a 10dB range. The first observation that falls out of these plots is that there exist two distributed noise sources, one right along the plume and the other is a reflection on the concrete test floor. It is obvious that any attempt to make free-field acoustic measurements in a horizontal rocket stand is corrupted by this reflection which nearly doubles the true amplitude.

Apart from the reflection issue, an interesting part of the noise source is the very long spatial extent, >30 diameter, that extends till the end of the visible afterburning core of the plume. At the lowest 960Hz the primary source and its reflection are merged; they become distinct at the next shown frequency of 2500Hz (Fig 8b). The quasi-periodic shock pattern of the plume is found to create periodic modulation of the noise source. As expected, the peak in the source distribution progressively moves closer to the nozzle exit with an increase in frequency; however, the downstream extent of the sources remained almost independent of frequency. At the highest shown frequency of 10kHz the sources become spotty and the side-lobes start to become visible. Further efforts are underway to improve the beamform process to diminish the influence of the side lobes.

Finally, figure 9 shows the application of the CLEAN-SC procedure to the conventional beamform maps. The outcome is somewhat disappointing: the long distributed sources are found to be converted into spotty blobs which may be unphysical.



Fig 5. Phased-array during a solid motor firing in a horizontal test stand.



Fig 6. Photograph of the plume by the camera at the center of the phased-array plate.

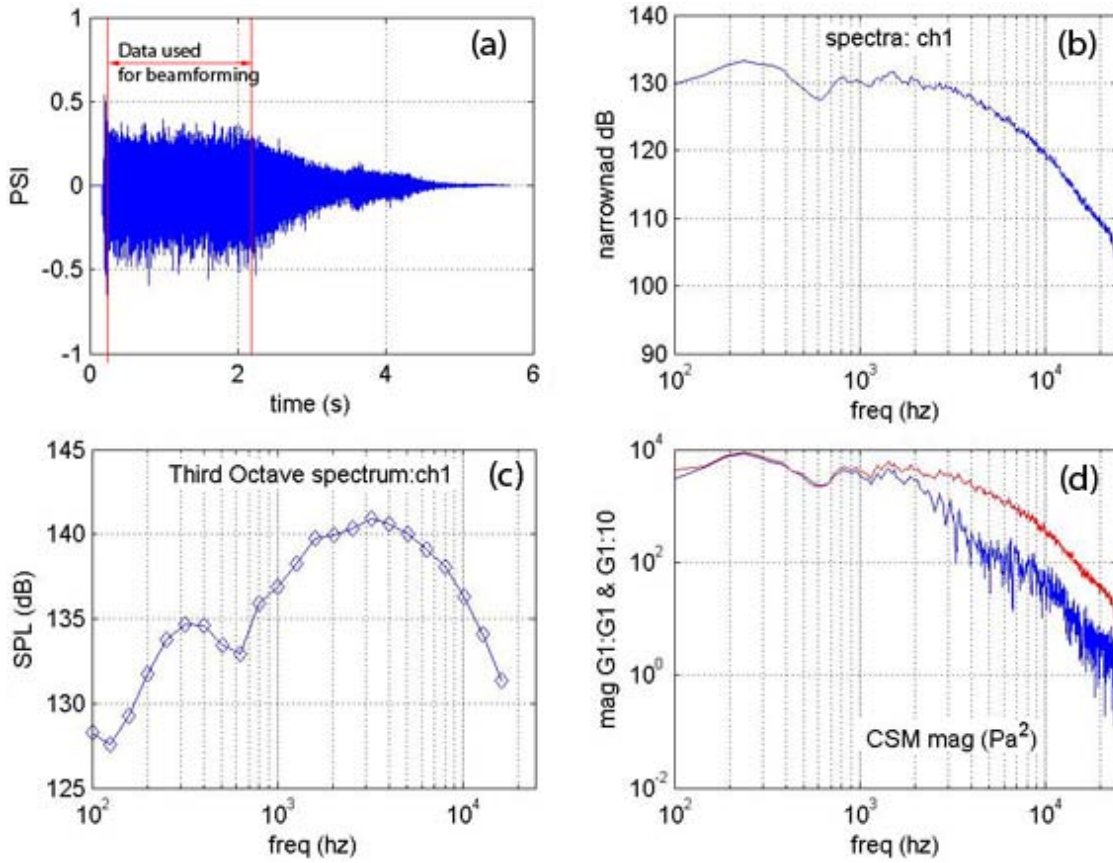


Fig 7. (a) Time trace of pressure fluctuations from one of the microphones; (b) narrow-band spectra; (c) third-octave spectra; (d) Magnitude of auto- and cross-spectra from indicated microphones.

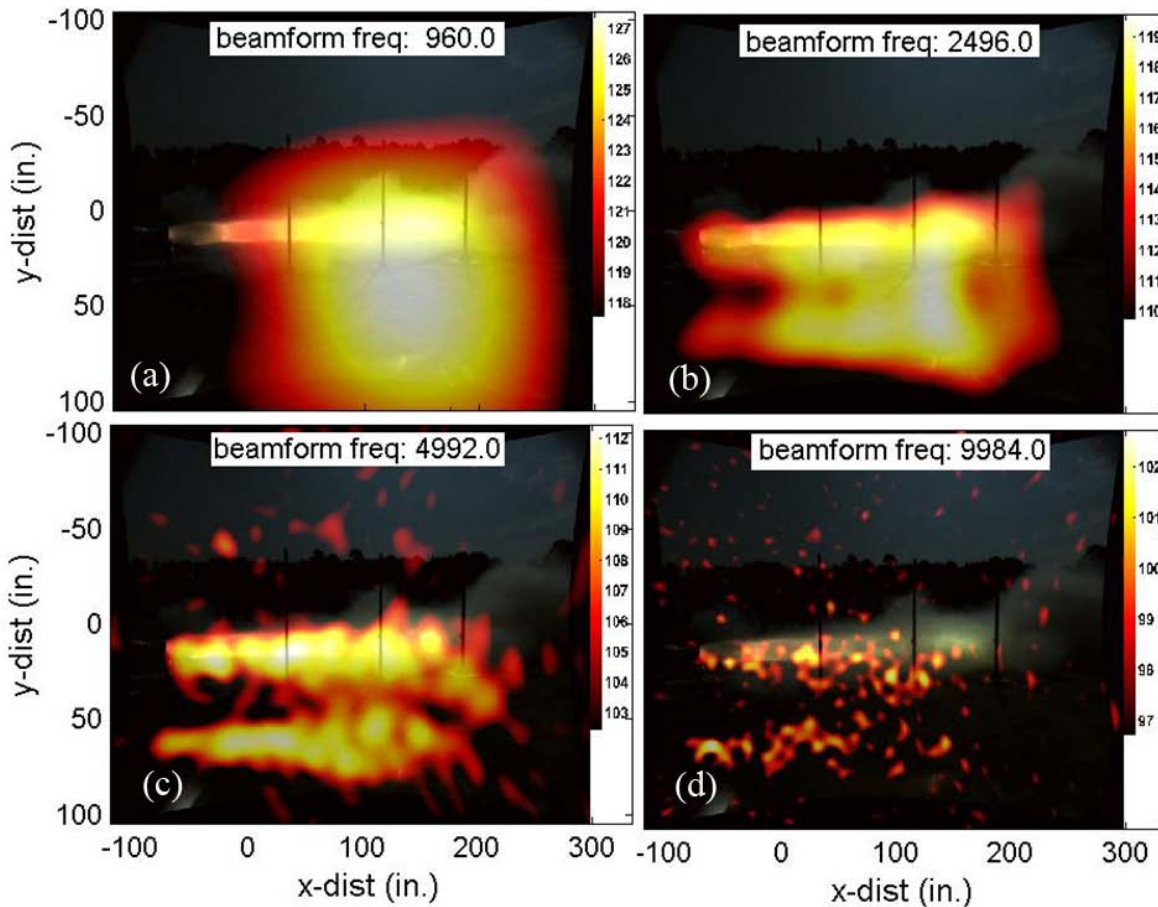


Fig 8. Conventional beamform image of the noise source distribution on the rocket plume at the indicated frequencies.

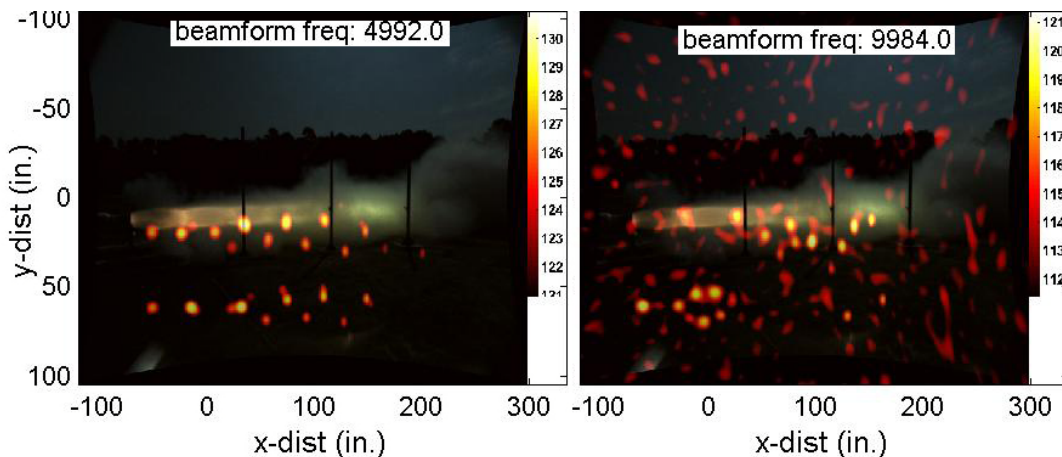


Fig 9. CLEAN-SC beamform images at the indicated frequencies.

V. SUMMARY AND CONCLUSION

A 70-element microphone array, made of $\frac{1}{4}$ inch condenser microphones, was used to image noise source distribution in the plume of a solid rocket motor. A part of the hardware was custom built for the test. Also the processing software was written afresh in the Matlab® platform. The existing array was ruggedized for use in an outdoor rocket test facility. There were four sets of protection applied: (a) an environment chamber was built to encase the array plate; (b) desiccants were placed inside the chamber; (c) the array chamber was continuously purged by dry air; (d) and finally a plastic rain cover was placed over the chamber. These protections were found to make all microphones survive a few thunderstorms and the shaking caused by the high noise level.

The array was first built and tested in the anechoic chamber of NASA Ames and then shipped to NASA Marshall for rebuilding around a horizontal rocket test stand. During the validation test in the anechoic chamber

the useful frequency range of the array was determined by a set of three speakers with variable separation. It was observed that the advanced beamforming routines such as CLEAN-SC, while significantly reduced the smearing associated with the point spread function, yet did not improve resolution beyond that set by the Rayleigh criteria. The image map created from the rocket plume showed very long coherent noise source modulated by the shock cells present in the plume. The future plan is to use the array to identify noise sources in a model scale lift-off acoustics test. Also, the computationally intensive DAMAS algorithm will be used to improve the noise source map. The noise source description collected from these tests will be compared with the existing model for launch acoustics.

Acknowledgement:

This work is supported by NASA Engineering Safety Center (NESC) technology development project TI-09-00597 with Mr. Roberto Garcia of NASA Marshall Space Flight Center as the technical monitor. We also acknowledge many useful suggestions from Dr. Clifton Horne and Mr. Nathan Burnside of Ames Research Center.

Reference:

¹Burnside, N. J., Jaeger, S. M., Reinero, B. R., Horne, W. C., & Soderman, P. T., 2002, "Array Design and Performance for a Large Scale Airframe Noise Study," AIAA paper 2002-2576.

²Underbrink, J. R. 2001, "Aeroacoustics Phased Array Testing in Low Speed Wind Tunnels," in *Aeroacoustics Measurements*, Springer, Ed. Thomas J. Mueller.

³Thomas F. Brooks* & William M. Humphreys, Jr., May, 2004 "A Deconvolution Approach for the Mapping of Acoustic Sources (DAMAS) Determined from Phased Microphone Arrays," 10th AIAA/CEAS Aeroacoustics Conference, Manchester, UK, AIAA-2004-2954.

⁴Robert. P. Dougherty*, Robert W. Stoker* "SIDELOBE SUPPRESSION FOR PHASED ARRAY AEROACOUSTIC MEASUREMENTS," AIAA-98-2242.

⁵Pieter Sijtsma, "CLEAN Based on Spatial Source Coherence," 13th AIAA/CEAS Aeroacoustics Conference 28th AIAA Aeroacoustics Conference) AIAA 2007-3436

⁶Dougherty, B., "DAMAS, Eigenvalues, CLEAN-SC and TIDY," keynote address, AIAA Aeroacoustics conference, May 2009

⁷Robert. P. Dougherty, Robert W. Stoker, 1998, "SIDELOBE SUPPRESSION FOR PHASED ARRAY AEROACOUSTIC MEASUREMENTS," AIAA-98-2242.

⁸Dougherty, R. P., Panda, J. & Lee, S. S. "Non-intrusive jet noise study combining Rayleigh scattering and phased array measurement techniques," AIAA 2005-2843, 2005.

⁹Lee, S. S. & Bridges, J., 2006, "Phased-Array Study of Dual-Flow Jet Noise: Effect of Nozzles & Mixers," AIAA 2006-2647.

¹⁰Horne, W. C., Burnside, N. J., Soderman, P. T., Jaeger, S. M., Reinero, B. R., James, K. D., Arledge, T. K., "Aeroacoustic Study of a 26%-Scale Semispan Model of a Boeing 777 Wing in the NASA Ames 40-by 80-Foot Wind Tunnel," NASA TP-2004-212802, 2004.